Lab on a Chip

PAPER

Cite this: *Lab Chip*, 2022, **22**, 1018

Imaging-guided bioreactor for de-epithelialization and long-term cultivation of *ex vivo* rat trachea†

Seyed Mohammad Mir,[a] Jiawen Chen,[a] Meghan R. Pinezich,[b] John D. O'Neill,[c] Sarah X. L. Huang,[d] Gordana Vunjak-Novakovic [b] and Jinho Kim *[a]

Recent synergistic advances in organ-on-chip and tissue engineering technologies offer opportunities to create *in vitro*-grown tissue or organ constructs that can faithfully recapitulate their *in vivo* counterparts. Such *in vitro* tissue or organ constructs can be utilized in multiple applications, including rapid drug screening, high-fidelity disease modeling, and precision medicine. Here, we report an imaging-guided bioreactor that allows *in situ* monitoring of the lumen of *ex vivo* airway tissues during controlled *in vitro* tissue manipulation and cultivation of isolated rat trachea. Using this platform, we demonstrated partial removal of the rat tracheal epithelium (*i.e.*, de-epithelialization) without disrupting the underlying subepithelial cells and extracellular matrix. Through different tissue evaluation assays, such as immunofluorescent staining, DNA/protein quantification, and electron beam microscopy, we showed that the epithelium of the tracheal lumen can be effectively removed with negligible disruption in the underlying tissue layers, such as cartilage and blood vessel. Notably, using a custom-built micro-optical imaging device integrated with the bioreactor, the trachea lumen was visualized at the cellular level, and removal of the endogenous epithelium and distribution of locally delivered exogenous cells were demonstrated *in situ*. Moreover, the de-epithelialized trachea supported on the bioreactor allowed attachment and growth of exogenous cells seeded topically on its denuded tissue surface. Collectively, the results suggest that our imaging-enabled rat trachea bioreactor and localized cell replacement method can facilitate creation of bioengineered *in vitro* airway tissue that can be used in different biomedical applications.

Received 6th December 2021,
Accepted 9th February 2022

DOI: 10.1039/d1lc01105g

rsc.li/loc

Introduction

Human conducting airways are lined by airway epithelium that mostly consists of multi-ciliated, club, goblet, and basal cells.[1–3] These airway epithelial cells collectively create a protective biophysical barrier between the external environment and underlying tissues against inhaled harmful substances, such as pathogens, allergens, chemical gases, or particulates.[4] The protective functions of the airway epithelium include mucociliary clearance,[5] tight junction formation,[6] and antimicrobial and anti-inflammatory secretions.[7] In addition to serving as the first line of defense of the lung, the airway epithelium is the prime site for the initiation and progression of many devastating respiratory disorders. For example, cystic fibrosis (CF), primary ciliary dyskinesia (PCD), and chronic obstructive pulmonary disease (COPD) are diseases caused by genetic mutations or environmental insults that primarily impact the airway epithelium, contributing to functional decline of the lung and ultimate end-stage lung diseases.[8–10] In CF patients, mutations in the cystic fibrosis transmembrane conductance regulator (CFTR) gene result in abnormal accumulation of viscous mucus within the airways and subsequent chronic airway infection and injury.[8,11] Moreover, PCD is caused by mutations of proteins involved in cilia structure, organization, and function, and it is characterized by chronic infection of the upper and lower airways due to ineffective airways clearance by ciliated cells.[9,12] Furthermore, the prolonged exposure of airway epithelium to noxious particles or gases can lead to COPD, accompanied by goblet cell hyperplasia, cell metaplasia, impaired ciliary function, mucus hypersecretion, and fibrotic tissue development.[10,13]

Recent synergistic advances in tissue engineering, biomaterials, and stem cell technologies have shown great potential for modeling different lung diseases,[14] repairing damaged tissues or organs,[15] studying human lung

[a] *Department of Biomedical Engineering, Stevens Institute of Technology, Hoboken, NJ, USA. E-mail: jkim6@stevens.edu*
[b] *Department of Biomedical Engineering, Columbia University, New York, NY, USA*
[c] *Department of Cell Biology, State University of New York Downstate Medical Center, Brooklyn, NY, USA*
[d] *Center for Stem Cell and Regenerative Medicine, University of Texas Health Science Center, Houston, TX, USA*

† Electronic supplementary information (ESI) available. See DOI: 10.1039/d1lc01105g

development,[16] and developing therapeutic materials without the use of animals.[17] For example, faithful *in vitro* models of diseases, such as cystic fibrosis,[18,19] COPD,[20] asthma,[21] surfactant protein B deficiency,[22] pulmonary fibrosis,[23,24] and viral infection,[25] have been generated using primary epithelial cells and induced pluripotent stem cells (iPSCs). Furthermore, recent establishment of innovative protocols for guided differentiation of airway stem cells, in particular basal cells,[26–28] allowed emergence of cell replacement therapy as a promising approach to repairing airway tissues of live patients that are severely injured or diseased beyond their intrinsic repairable limits,[29] or donor lungs that are refused for transplantation due to substantial tissue damage.[30]

To study differentiation and therapeutic functionality of airway stem cells, various *in vitro* platforms have been created and used. Traditionally, airway stem cells have been cultured and assessed in a static two-dimensional (2D) environment of a petri dish or transwell insert that can provide controllable cell culture conditions.[31–33] The 2D-cultured cell monolayer enabled fundamental studies related to cell signaling pathways, cellular responses, and cell differentiation.[34,35] Notably, lung-on-a-chip (LOC) devices with lung-mimetic designs have been developed that can allow co-culturing of different lung cells in an environment where fluids (*e.g.*, air and culture media) are dynamically manipulated.[36] For instance, airway epithelium and endothelium were cultured on the apical and basal sides of a porous membrane, respectively, to mimic breathing airway, allowing *in vitro* drug screening and disease modeling.[37–39] However, these *in vitro* platforms are incapable of recapitulating the complex three-dimensional (3D) architecture and dynamic cell–matrix interactions found *in vivo*, resulting in considerable differences between 2D-cultured cells and *in vivo* cells in terms of morphology, proliferation, and differentiation.[40,41]

Decellularized allogeneic or xenogeneic tissue grafts have been used to provide *in vivo*-like microenvironments to the airway epithelial cells or stem cells during cell culture.[42,43] For example, isolated rat or mouse tracheas with their endogenous cellular components completely removed *via* repeated freezing and thawing or chemical treatments were seeded with airway cells.[44,45] When the cell-seeded decellularized airway tissues were implanted subcutaneously into immunodeficient host animals,[43] functional airway epithelial layer was regenerated on the luminal surface of the tissues. The *in vivo* cultured tissue-specific scaffolds allowed study of stem cell differentiation and confirmed regenerative capacity of the airway stem cells.[46] Because cell-seeded tissue scaffolds are embedded in the host body, however, major limitations of this tissue culture approach include lack of ability for rapid manipulation of the cell culture conditions and *in situ* monitoring of the cellular responses. In particular, creation of the air–liquid interface and time-dependent supply of growth factors or cytokines that are essential for stem cell differentiation are difficult to achieve in the *in vivo*-cultured tissue scaffolds.[47] Further, different from *in vitro* models, microscopic assessments of the cultured cells are only possible after removing the cell–tissue constructs from the host after completion of each experiment.[44,48]

Here, we report an imaging-enabled bioreactor system that allows long-term *in vitro* cultivation of isolated rat trachea and direct visualization of the tracheal lumen at the cellular level (Fig. 1). Using this platform, we demonstrated partial removal of the epithelial layer from the trachea lumen without disrupting the underlying tissue layers and extracellular matrix (ECM) components, onto which exogeneous airway cells or stem cells could be implanted to restore functional epithelium. Further, we created a micro-imaging device that can be inserted into the inner space of the *in vitro*-cultured trachea to allow *in situ* visual monitoring of the cell replacement and cultivation. Notably, the de-epithelialized rat tracheas supported survival of exogenous cells, such as mesenchymal stem cells (MSCs), that were topically seeded onto the denuded tracheal lumen. We envision that the imaging-enabled bioreactor platform and tissue manipulation methodology established in this study could enable creation of humanized airway tissues by combining with human airway stem cells, allowing *in vitro* study of airway diseases and expediting development of therapeutics and intervention modalities.

Results

Imaging-enabled bioreactor for *in vitro* cultivation of isolated rat trachea

We constructed an imaging-enabled bioreactor system that enabled partial removal of the epithelium and long-term culture of the tracheal tissue (Fig. 1A and S1, Table S1†). The bioreactor was designed and constructed in a way that the luminal surface of the trachea can be treated using different solutions (*e.g.*, decellularization solution, washing solution, cells, culture medium) while the entire trachea is submerged in a cell culture medium to maintain the viability of the trachea tissue during planned experiments (Fig. 1B and C). Using this system, isolated rat trachea can be de-epithelialized by introducing decellularization reagents (*i.e.*, sodium dodecyl sulfate detergent; SDS) with specified volumes and concentrations directly into the inner space of the trachea. Disrupted cells can be removed from the tissue surface with phosphate-buffered saline (PBS) washing solution. The airway imaging device integrated into the bioreactor enables direct *in situ* visual inspection of the trachea lumen in both bright-field and fluorescence modes.

De-epithelialization of *ex vivo* rat trachea

To remove the epithelial layer from the trachea without disrupting the rest of the underlying airway tissue (Fig. 1D), a thin layer of 2% or 4% SDS detergent was deposited topically onto the tracheal lumen by instilling a small volume (50 μL) of the detergent solution. Intratracheal instillation of a small

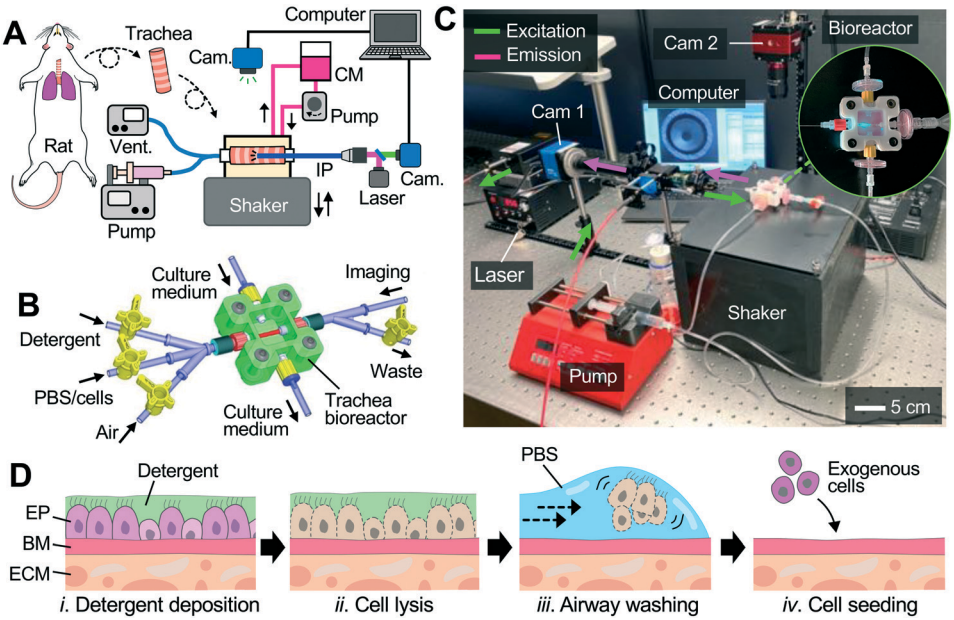

Fig. 1 Overview of imaging-enabled bioreactor and de-epithelialization of *ex vivo* rat trachea: (A) schematic of the imaging-integrated rat trachea bioreactor platform. Cam: camera. CM: culture medium. IP: imaging probe. Vent: ventilation. (B) Three-dimensional (3D) representation of the trachea bioreactor. (C) Photograph of the bioreactor system. Cam: camera. (D) Schematic showing the procedure of de-epithelialization of rat trachea. EP: epithelium. BM: basement membrane. ECM: extracellular matrix. PBS: phosphate-buffered saline.

volume of liquid (*e.g.*, aqueous solution) through the respiratory tract can generate a thin layer of the liquid onto the airway lumen.[49–51] Following disruption of the epithelium through detergent exposure, the lysed cells were then cleared from the trachea by washing with PBS buffer while the entire trachea was vibrated mechanically using our custom-built shaker (Fig. S2†). In particular, the trachea was oscillated at 20 Hz with a vertical displacement of approximately 0.3 mm (Videos S1 and S2†). Exogeneous cells (*e.g.*, airway epithelial or stem cells) can be seeded onto the denuded tracheal lumen to reconstitute the epithelium within the bioreactor.

In situ visualization of the trachea lumen

We used our custom-built *in situ* airway imaging device to inspect the luminal surface of the rat trachea tissue during *in vitro* cell removal (Fig. 2A, i–iii). We used a 1951 USAF (U.S. Air Force) test target to evaluate the resolution of the images obtained using the device. The images were acquired in air, and they showed high resolution and good quality with approximately 5 μm of the smallest features resolvable (Fig. 2A, iv). To visualize the trachea lumen, the imaging probe was directly inserted into the trachea through a cannula connected to the trachea (Fig. 2B, i and ii

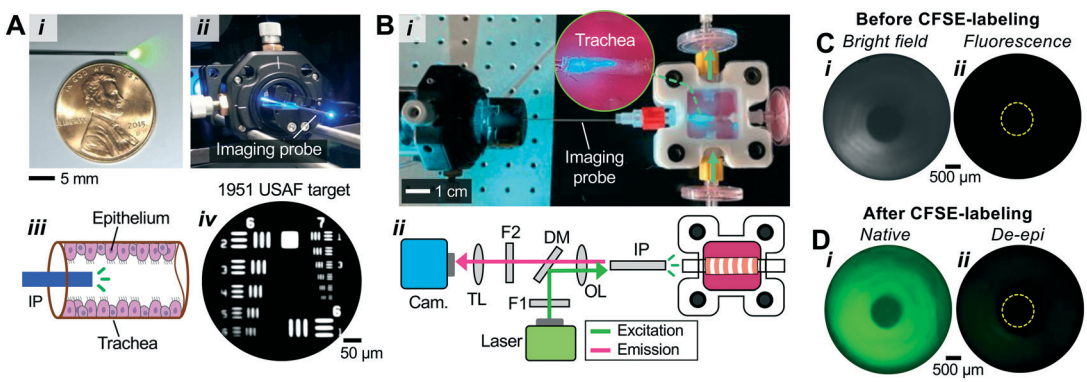

Fig. 2 *In situ* visualization of the trachea lumen using custom-built micro-optical imaging device: (A) (i–iii) GRIN lens (diameter: 500 μm) used for both bright-field and fluorescence imaging of the rat tracheal lumen. (iv) 1951 USAF test target imaged using the imaging device. (B) (i) Photograph and (ii) schematic showing the imaging probe being used for visual inspection of an *in vitro*-cultured rat trachea. Cam: camera. TL: tube lens. F: optical filter. DM: dichroic mirror. OL: objective lens. IP: imaging probe. (C) (i) Bright-field and (ii) fluorescence images of the interior of the rat trachea before CFSE-labelling of the epithelium. (D) Fluorescence images of (i) native and (ii) de-epithelialized (De-epi) rat trachea lumen that was labelled with CFSE.

and S3†). Both bright-field (Fig. 2C, i; Video S3†) and fluorescence images (Fig. 2C, ii) of the local luminal surface were obtained, respectively, by using white light and 488 nm laser for illumination prior to carboxyfluorescein succinimidyl ester (CFSE) labeling of the epithelial layer. While no fluorescence signal was observed before labeling, a discernible signal (*i.e.*, green light) was observed when the epithelium was labeled with CFSE (Fig. 2D, i and Video S4†). Notably, following de-epithelialization, the intensity of the fluorescent signal substantially decreased, indicating clearance of the epithelium from the tracheal lumen (Fig. 2D, ii). This result highlights the utility of our imaging approach in *in situ* and minimally invasive monitoring of the epithelium removal.

Partial removal of tracheal epithelium with preserved tissue ECM

Histological evaluation of de-epithelialized tracheas showed complete removal of the epithelium across the luminal surface of de-epithelialized tracheas treated with 2% and 4% detergent solutions (Fig. 3). In particular, high magnification of H&E images confirmed the removal of the pseudostratified columnar epithelium from the trachea mucosa and preservation of other cells in the submucosa, cartilaginous, and adventitia layers (Fig. 3A). Further, histological imaging analysis of the airway tissues treated with SDS detergent showed that the epithelial layer was completely and uniformly detached and removed across the entire airway luminal surface regardless of the location (Fig. S4–S7†). The structure pattern of the tissue layers and endogenous cells, such as cartilage and chondrocytes, underneath the basement membrane was well preserved following de-epithelialization. Similarly, pentachrome (Fig. 3B) and trichrome (Fig. 3C) staining revealed maintenance of the tissue architecture and ECM components, including collagen and proteoglycans (*e.g.*, mucins), while the airway epithelium was cleared from the lumen.

Further, we confirmed the preservation of ECM components of the de-epithelialized tracheas *via* immunofluorescence staining. Immunostaining of the trachea tissues by epithelial cell adhesion molecule (EpCAM) and 4′,6-diamidino-2-phenylindole (DAPI) revealed removal of the epithelial layer as no EpCAM (green) and DAPI (blue) signals were detected at the lumen of the trachea (Fig. 4A). De-epithelialized tracheas treated with 4% SDS showed a reduction in the DAPI signal throughout the tissue, suggesting potential disruptions occurred to endogenous subepithelial cells due to increased detergent concentration. Nevertheless, the de-epithelialization method preserved laminin (green) (Fig. 4B), collagen I, elastin, and smooth

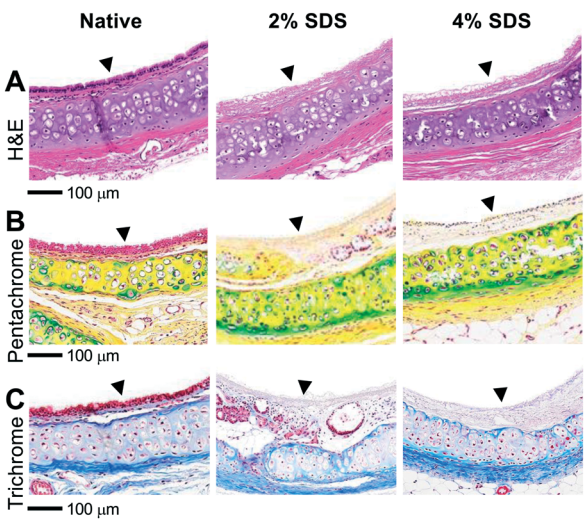

Fig. 3 Histologic analysis of native and de-epithelialized rat tracheas: (A) H&E, (B) pentachrome, and (C) trichrome staining images of native and de-epithelialized rat tracheas with 2% and 4% SDS. The images of de-epithelialized tracheas show removal of the epithelium and preservation of ECM architecture. *Pentachrome: purple (cell cytoplasm), blue (cell nuclei), green (proteoglycans), yellow (collagen fibers). *Trichrome: pink (cell cytoplasm), dark blue (cell nuclei), blue (collagen). Arrowhead: tracheal lumen.

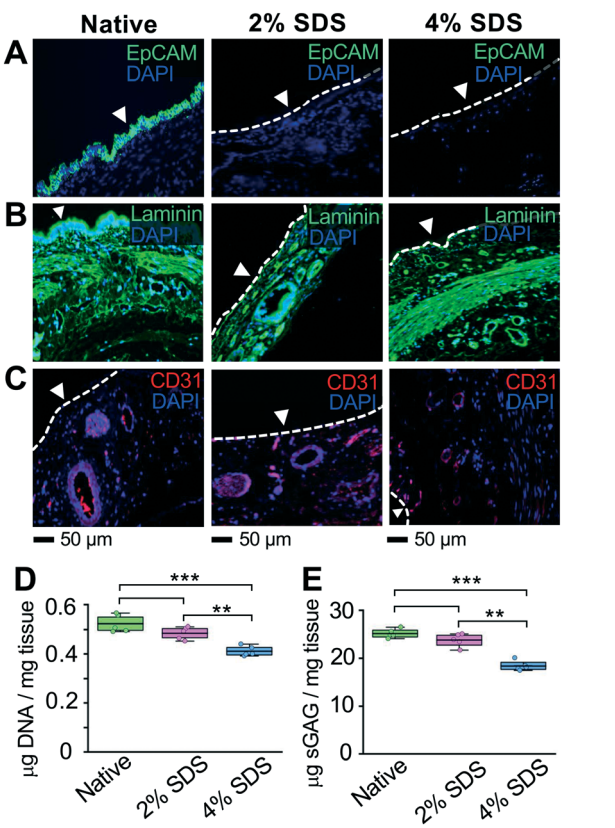

Fig. 4 Evaluation of ECM components *via* immunohistochemistry and DNA/GAG quantification: immunostaining images of (A) epithelial cell adhesion molecule (EpCAM), (B) laminin, and (C) cluster differentiation 31 (CD31) showing removal of the tracheal epithelium and preservation of ECM components within the rat trachea treated with 2% and 4% SDS. Arrowhead: tracheal lumen. (D) DNA and (E) GAG quantifications (n = 5 each) decrease in DNA and sulfated GAG amounts. Error bars represent means ± SD of experimental values. **$p < 0.01$. ***$p < 0.001$.

muscles of the trachea tissue (Fig. S8†). Furthermore, immunostaining of the de-epithelialized tissues with endothelial cell marker (cluster of differentiation 31; CD31) confirmed that the blood vessels of the tissue remained intact (Fig. 4C).

DNA quantification showed no significant differences between native tissues (0.52 ± 0.03 μg mg^{-1} of tissue) and de-epithelialized tracheas treated with 2% SDS (0.48 ± 0.03 μg mg^{-1} of tissue; $p = 0.11$) (Fig. 4D). On the other hand, the DNA content decreased by nearly 21% in the tracheas treated with 4% SDS (0.41 ± 0.02 μg mg^{-1} of tissue; $p < 0.001$), indicating some of the endogenous cells were affected when the trachea tissues were exposed to the higher concentration of the detergent solution. Furthermore, we quantified the glycosaminoglycans (GAGs) in the tissues as GAGs play important roles in growth, differentiation, and function of resident cells (Fig. 4E). GAGs are known to regulate cell signaling, growth, proliferation, and differentiation by acting as a bridge between receptors and ligands that modulate signaling between cells.[52] GAGs can regulate ECM organization and remodeling by binding to collagen and elastin fibers.[53] Further, GAG molecules maintain viscoelastic mechanical properties of tissue that are important in tissue homeostasis.[54] Our GAG quantification results revealed no significant difference in sulfated GAG content between native trachea (25.2 ± 0.9 μg mg^{-1} tissue) and de-epithelialized tracheas treated with 2% SDS solution (23.8 ± 1.4 μg mg^{-1} of tissue; $p = 0.17$).

However, similar to DAPI staining and DNA quantification, nearly a 27% decrease in the sulfated GAGs was observed in the tracheas treated with 4% SDS solution (18.4 ± 1.0 μg mg^{-1} of tissue; $p < 0.001$).

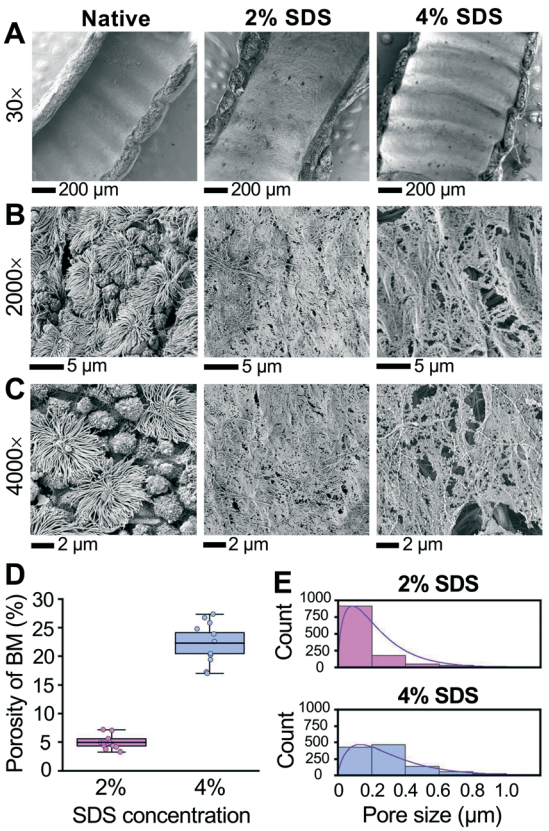

Fig. 5 Investigation of the luminal surface of de-epithelialized tracheas *via* SEM imaging: SEM images obtained at (A) 30×, (B) 2000×, and (C) 4000× of magnifications showing the luminal surface of the *ex vivo* rat tracheas. (D) Porosity of basement membrane (BM) of de-epithelialized tracheas treated with 2% and 4% SDS. (E) Size distribution of pores generated in the BM following the SDS treatment.

Scanning electron microscopy (SEM) imaging of the tracheal lumen

We then investigated topological changes in the luminal surfaces of de-epithelialized trachea *via* SEM imaging where the images were obtained at different magnifications (30× in Fig. 5A; 2000× in Fig. 5B; and 4000× in Fig. 5C). The native trachea showed that the luminal surface was densely populated by different epithelial cells, predominantly multi-ciliated and goblet cells. On the other hand, the SEM images of de-epithelialized tracheas with 2% and 4% SDS showed absence of the tracheal epithelium. Notably, in both de-epithelialized trachea lumen surfaces, a thin membrane layer, which is most likely the basement membrane, and mesh network of airway ECM were clearly visible. Structural disruption of the basement membrane and tissue ECM was more prominent in the tracheas treated with 4% SDS compared with that of 2% SDS as the porosity of the remaining ECM structure increased with the concentration of the SDS. Quantitative analyses of the SEM images showed that porosity of the basement membrane of the tracheas treated with 2% SDS detergent film was approximately 4.9 ± 1.2% while the sizes of the pores were mostly smaller than 0.2 μm (nearly 76% of total pores). On the other hand, porosity of the basement membrane exposed to 4% SDS film (porosity: 22.3 ± 3.7%) was 4.5 times greater than that of the basement membrane exposed to 2% SDS and nearly 80% of the total pores were smaller than 0.4 μm. The pore analysis results suggest the correlation between the detergent strength and the physical disruption induced to the airway tissue (Fig. 5D and E). Notably, use of mechanical vibration during the airway washing facilitated detachment of the epithelium as SDS-disrupted epithelium remained attached onto the lumen surface when no vibration was applied to the tissue (Fig. S9†). This result clearly indicated that oscillation energy provided to the trachea in the presence of the shear flow promoted disruption and detachment of the detergent-lysed cells from the airway tissue ECM.

Evaluation of chondrocyte viability and cytotoxicity of the de-epithelialized trachea tissue

We assessed the viability of chondrocytes in native and de-epithelialized tracheas after culturing for two weeks in the bioreactor. We used the de-epithelialized trachea treated with 4% SDS solution, which is the maximum concentration of

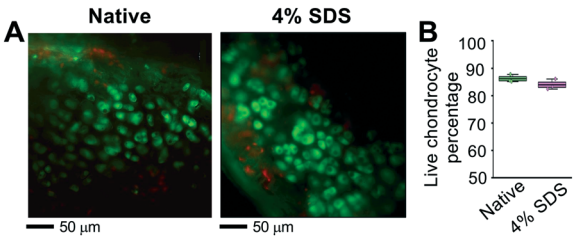

Fig. 6 Live and dead analysis of native and de-epithelialized trachea (4% SDS): (A) fluorescent images of live and dead cartilage cells obtained *via* conventional fluorescence microscopy showing the viability of chondrocytes after de-epithelialization and two weeks of *in vitro* cultivation. (B) Quantification of the viable chondrocyte revealed that there was no significant difference between native and de-epithelialized tracheas (p = 0.18).

SDS used in this study. The fluorescent images of the trachea sections obtained using a conventional fluorescent microscope revealed that most of the chondrocytes seeded onto native and de-epithelialized tracheas survived following two weeks of the *in vitro* cultivation (Fig. 6A). In addition, quantification of viable cartilage cells (green) and the dead cells (red) showed that both native (86.2% ± 1.4%) and de-epithelialized (84% ± 1.8%) tracheas maintained the viability of majority of the cartilage cells (Fig. 6B).

We also investigated whether the SDS-treated tracheas can support attachment, growth, and proliferation of exogenous cells seeded on the lumen surface without generating a cytotoxic environment. To do this, CFSE-labelled MSCs were introduced and topically deposited onto the inner space of *ex vivo* rat tracheas with their epithelium removed *via* 4% SDS (Fig. 7). Using MSCs labeled with red quantum dots, we evaluated the imaging resolution of our GRIN lens imaging probe (Fig. 7A). The fluorescent images acquired showed that individual cells could be visualized using our imaging device. We then monitored cells seeded into the isolated rat trachea. Immediately after cell seeding, the micro-imaging probe was inserted into the trachea to confirm the deposition of the cells (green) onto the de-epithelialized tracheal lumen (Fig. 7B, i–iii). Notably, distribution of the seeded cells across the airway lumen was not uniform as the cells tend to accumulate onto the bottom half of the airway. In our previous studies, we determined that this is due to weak adhesion and engraftment of the cells onto the airway surface due to gravity.[49,50] Homogeneous cell distribution can be achieved by introducing the cells *via* a viscous medium, such as collagen hydrogel solution.[55] The bioreactor containing the cell-seeded trachea was then transferred to an incubator and connected to the perfusion pumps for extended *in vitro* culture (*i.e.*, 1, 4, and 7 days) (Fig. 7C and D and S10†). The fluorescent images of the MSCs cultured on the de-epithelialized tracheal lumen were obtained *via* a conventional fluorescent microscopy. The imaging results showed that the density of the cells covering the surface gradually increased over time (*i.e.*, day 1: 15.6 ± 6.1 cells mm^{-2}, day 4: 94.6 ± 15.1 cells mm^{-2}, day 7: 145 ± 12.1 cells mm^{-2}; Fig. 7E, i–iv). Further, the average

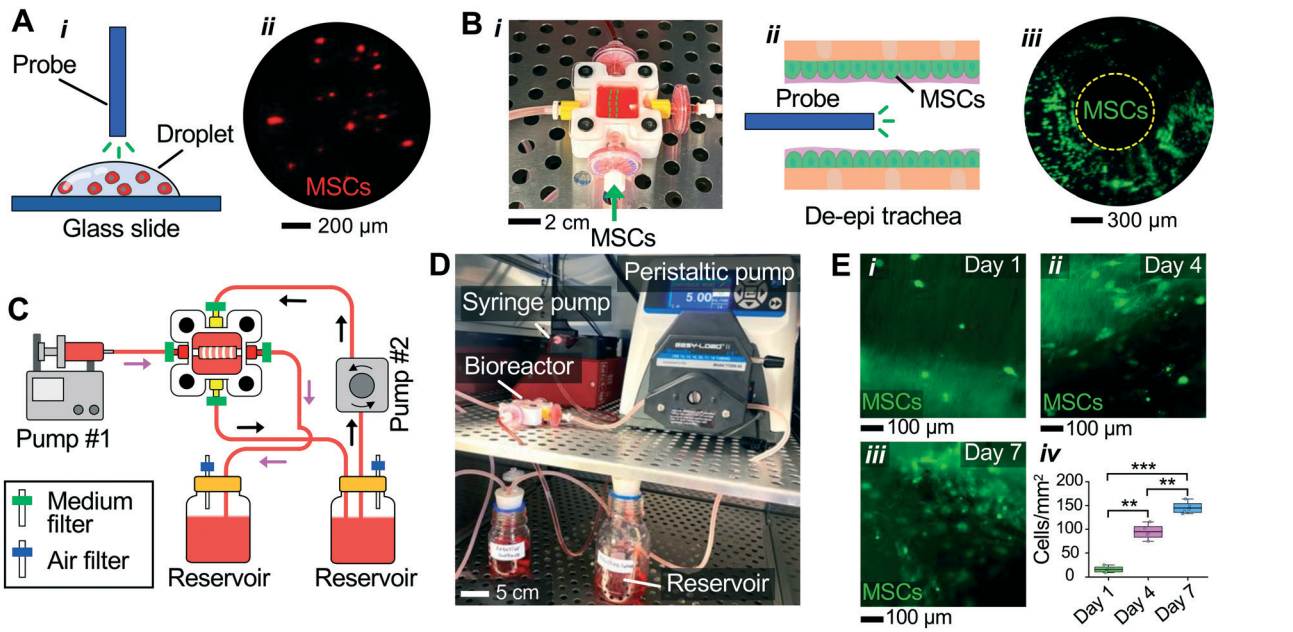

Fig. 7 Evaluation of cytotoxicity of the rat tracheas de-epithelialized *via* 4% SDS detergent: (A) characterization of the GRIN lens imaging probe using MSCs (red) labeled with quantum dots and suspended in culture medium. (B) (i–iii) CFSE-labelled MSCs (green) were deposited onto the denuded rat trachea lumen using the GRIN lens imaging device. (C) Schematic and (D) photograph showing the experimental setup used for long-term *in vitro* culture (*i.e.*, over one week) of MSC-seeded de-epithelialized rat tracheas. Arrows show flow directions. (E) (i–iii) Fluorescence images of CFSE-labelled MSCs (green) being cultured on the tissue surface over the course of 7 days. The fluorescence images were obtained using a conventional microscope. (iv) Density of the cells measured at different time points. Error bars represent means ± SD of experimental values. **p < 0.001. ***p < 0.0001.

circularity of the seeded cells, which is a normalized ratio of area to perimeter of the cells, was calculated to quantitatively evaluate attachment and engraftment of the cells on the surface. Analysis showed that cell circularity decreased over time, confirming active binding and incorporation of the cells onto the de-epithelialized tracheal lumen (*i.e.*, day 1: 0.90 ± 0.07, day 4: 0.22 ± 0.04, day 7: 0.25 ± 0.08; Fig. S11†). Notably, SEM imaging showed that seeded MSCs quickly initiated binding onto de-epithelialized lumen at day 1 as multiple protrusions extending from the cell membrane to the tissue surface were observed (Fig. S12†). Collectively, the results indicated that the de-epithelialized trachea lumen provided a suitable microenvironment that allowed engraftment, survival, and proliferation of topically seeded new cells.

Discussion

To promote survival, proliferation, and differentiation of implanted exogenous cells, preservation of the underlying ECM structure and components within decellularized tissue is critical. The ECM provides biochemical and mechanical cues as well as suitable physical environments that are essential for tissue- or organ-specific cellular responses and activities.[56–59] Recent studies demonstrated that airway basal stem cells implanted into decellularized trachea tissues are able to reconstitute a wide range of airway epithelial cell types, including multi-ciliated and secretory cells, that were difficult to achieve using traditional 2D cell culture platforms.[26,28,42,47] On the other hand, the limitations of existing methods of culturing stem cell-implanted airway scaffolds include lack of methods to precisely modulate cell culture conditions and rapidly evaluate the behaviour and responses of implanted cells. Because cell-seeded tissue scaffolds are typically implanted in the host animal's body during the culture, controlling and monitoring the cells and tissues *in situ* are very challenging.[60,61] Also, existing decellularization protocols focus on the complete removal of all existing cellular components from the airway tissues (*e.g.*, epithelium, endothelium, stromal cells, *etc.*), which eliminates the possibility of investigating interactions between resident subepithelial cells and newly implanted stem cells.[62–64]

In this work, we developed an imaging-enabled bioreactor platform that allows long-term culture (at least one week) of cell-implanted rat trachea in a precisely modulated *in vitro* environment (Fig. 1). The concept and design of our bioreactor are similar to those of innovative flow-controlled *in vitro* cell or tissue culture platforms.[65,66] This platform is capable of: (i) applying user-defined biochemical treatments to *ex vivo* airway tissue; (ii) *in situ* monitoring of the interior surface of the airway at the cellular level; and (iii) long-term culturing of *ex vivo* tissues following topical seeding of exogenous cells. Further, we developed a tissue-manipulation protocol that permitted partial removal of the epithelium of the trachea lumen while preserving the rest of the tissue layers and ECM components. This targeted epithelium removal approach utilizes topical deposition of a liquid solution containing decellularization reagents (*e.g.*, detergent solution) directly onto the airway lumen. By modulating the decellularization reaction time and detergent strength, the epithelium can be dislodged and removed with washing solution under mechanical vibration. Vibration-assisted airway washing used in our study can further reduce the detergent amount and reaction time needed to lyse the epithelium, minimizing detergent-induced damage and detergent residue within the ECM.

Using this innovative platform and protocol, we demonstrated imaging-guided removal of the epithelial layer from the lumen of isolated rat trachea where fluorescently labeled epithelium was effectively ablated from the tissue surface. Notably, the cell removal was monitored visually *in situ* using our custom-built imaging device incorporated into the bioreactor (Fig. 2). We further confirmed the partial epithelium removal through additional tissue assessment methods, including histology, immunostaining, DNA/protein quantification, and electron beam microscopy (Fig. 3–5). All tissue evaluation results consistently indicated that the tracheal epithelium could be ablated while the ECM components and the rest of the cells underneath the basement membrane of the treated trachea could be preserved using our targeted epithelium removal approach. Higher concentration of detergent (4% SDS *vs.* 2% SDS) appeared to increase disruption in the ECM slightly. The rat tracheas treated with 4% SDS, compared with the tracheas treated with 2% SDS, resulted in the decreased number of subepithelial cells (Fig. 4A), reduced amounts of DNA and GAGs (Fig. 4B), while ECM structure became more porous (Fig. 5). Nevertheless, long-term cell culture experiments showed that rat tracheas de-epithelialized using 4% SDS detergent preserved most of the cartilage cells and were able to support active engraftment and proliferation of exogenous MSCs seeded onto the ECM surface (Fig. 6 and 7).

In this study, a thin liquid film of detergent was created topically onto the tracheal lumen by instilling a small volume of SDS detergent solution. By simply modulating detergent concentration and potentially exposure time, we demonstrated that the epithelium could be lysed by the detergent film and cleared from the tracheal lumen *via* vibration-assisted airway wash without damaging the rest of the tissue matrix components underneath the basement membrane. While "flooding" the airspace of the trachea with the detergent solution could also allow de-epithelialization, our "thin film-based approach" can provide important benefits, including small amounts of reagents required, usage of *in situ* tissue monitoring, and its translational potential. First, the thin film method requires a small volume (less than 50 μL) of reagents, such as SDS detergent used in this study, for epithelium removal, while the flooding method would require much larger reagent volumes (at least ~300 μL) to fill the airspace. Reduced amounts of reagents required can allow cost-effective airway tissue manipulation. Second, when the airway lumen is coated with detergent

solution, visual inspection of the airway surface using a locally placed GRIN lens becomes easier than that of flooded airway following each step during the epithelium removal process (*e.g.*, cell labeling, detergent film deposition, airway wash, and de-epithelialization inspection). Inserting the imaging probe into liquid-filled airspace and imaging through the liquid medium are challenging within the flooded airway. Third, the thin film-based method could be more readily translated into clinics to treat patient's pathologic airway tissues when combined with innovative regenerative medicine technologies. For example, diseased or damaged epithelium could be removed from the airway lumen *via* the thin film approach and replaced with *in vitro*-grown healthy primary airway epithelial cells or stem cells to regenerate the native epithelial layer within the patient's lung. On the other hand, the flooding method could cause substantial lung tissue damage as it does not permit localized and controllable reagent delivery within the geometrically complex respiratory tract.

Conventional imaging-based tissue analysis methods, such as histology, immunohistochemistry, and electron beam microscopy, require removal of tissue samples from the airway for microscopic analysis. This tissue sampling and imaging modalities are time consuming, resource intensive, and destructive to the tissue. On the other hand, our *in situ* airway imaging using the GRIN lens probe allows rapid and non-destructive visual monitoring of the airway lumen at both tissue and cell levels. Further, the rat tracheal tissue is not transparent, and thus it is difficult to image the airway lumen from the outside. While the excitation laser light (wavelength: 488 nm) still can penetrate and diffuse through the thin trachea wall (thickness: ~300 μm)[67] (Fig. 2B, i), emission light generated by individual airway epithelial cells are difficult to resolve externally. The imaging probe was mainly used to evaluate the outcomes of epithelium removal and cell implantation in this study. However, potential benefits of this *in situ* imaging modality are substantial as it can permit direct and live visualization of local airway tissues and cells during investigation of their responses and functions under different local microenvironments provided. The ability to evaluate and modulate the cellular behaviors and responses rapidly and minimally invasively can improve our understanding of the relationship between tissue structure and physiological functions.[68,69]

In this study, *in situ* imaging was performed at specified time intervals to visually inspect the airway lumen or seeded cells. On the other hand, the ability to monitor the airway tissues and cells in real time during the epithelium removal, replacement, and regeneration could offer significant benefits. For example, real-time monitoring of implanted cells over time would provide visually based information related to transient cellular events and responses that could be otherwise missed in periodic or end-point assays. Thus, real-time cell imaging could allow tight regulation of the microenvironment required for the implanted cells, such as airway epithelial stem cells, to restore the functional epithelium. In addition, imaging the cells in real time in their natural states could reduce artifacts that could be introduced in other imaging modalities during tissue processing steps, such as tissue fixation and immunostaining.[70]

Our *in situ* imaging approach and the bioreactor can be modified to allow real-time monitoring of different steps involving de-epithelialization and cell cultivation processes. For example, the fluorescent signals generated by the CFSE-labeled epithelium can be monitored and quantified continuously over time during the de-epithelialization to more accurately determine the optimal exposure time of the epithelium to the SDS detergent. Further, while it was not demonstrated in this study, live imaging of migration of exogeneous cells seeded onto the tracheal lumen could provide invaluable information about the contributions of the cell seeding density on the speed of functional epithelium regeneration.

In partial de-epithelialization, controlling the exposure time and detergent concentration are the major driving factors which can modulate the penetration depth and reaction of the detergent molecules within the airway tissue.[71,72] To our best knowledge, our current study is the first one that demonstrates partial removal of the airway epithelium without damaging the subepithelial tissue structure *via* topically deposited detergent film. Further investigation on the contribution of detergent exposure duration on the decellularization process can provide more complete understanding of the detergent film-based de-epithelialization modality.

To obtain reliable and repeatable study outcomes, it is important to establish leak-free connection at both ends of the trachea. In all experiments that we performed, no leakage of CFSE or fluorescently labeled cells from the interior to the exterior of the trachea was observed. This suggests that leak-free connection was created at both tracheal ends. On the other hand, any leakage could be further confirmed by instilling culture media added with fluorescent tracers through the inner space of the trachea. In this approach, failed connection between the trachea and cannulas would be indicated by presence of the tracers in the external media which can be quantified by measuring the fluorescent intensity of the tracers *via* spectrophotometry or fluorescent microscopy.

It would be intriguing to investigate the viability of the tracheal tissue regions that were not treated with detergent and implanted with exogenous cells. Confirming the viability of these tissue regions could help us further confirm the functionality of the bioreactor in *in vitro* support of airway tissues. Nevertheless, viability of the cartilage cells and topically seeded MSCs in the central regions of the tracheas following long-term cultivation suggest that native airway tissues could remain viable and functional when they are cultivated within our bioreactor.

The experimental results suggested that our imaging-enabled rat trachea bioreactor can allow the creation of

bioengineered trachea tissue constructs. It is important to show the de-epithelialized airway tissue grafts generated *via* SDS film treatment do not have adverse effects on the cellular functions. The main goal of the cell engraftment and proliferation study using topically implanted MSCs is to evaluate whether the SDS molecules that may remain in the tissue scaffolds following the de-epithelialization process generate a cytotoxic environment to the implanted cells during *in vitro* culture. While MSCs were used to evaluate the cytotoxicity of the SDS-treated airway tissues, the use of *in vitro*-grown airway epithelial cells or stem cells could confirm whether the de-epithelialized tissues can promote cell differentiation, interactions, and function regeneration. For example, in future studies, human airway basal stem cells can be implanted onto de-epithelialized rat tracheas to reconstitute functional epithelium using our platform to generate *in vitro* humanized airway tissues. Such humanized airway constructs could potentially be used to investigate human airway diseases, screen therapeutics, and study human stem cell differentiation without the need of costly immunodeficient animals that are difficult to maintain and manipulate.

While it was not demonstrated in this current study, the trachea could be supplied with a gas flow (*e.g.*, air) to provide *in vivo*-like flow shear stress to the seeded cells or culture medium to create an air–liquid interface (ALI) within the trachea. For example, creation of *in vivo*-like shear stress above the seeded cell layer can be achieved by ventilating the trachea with a small animal ventilator (*e.g.*, PhysioSuite, Kent Scientific; tidal volume: 15 mL kg^{-1} of animal weight; breathing rate: 60–70 breaths per minute).[73,74] In addition, future studies should evaluate the creation of the ALI within the cultured trachea in our bioreactor to guide the differentiation of implanted basal cells into different epithelial cell types. The creation of ALI can be achieved by selectively controlling the infusion of culture medium and airflow through dedicated inlet ports. To create the ALI, a small volume (*e.g.*, 50 μL) of culture medium can be periodically introduced through the inner space of the trachea. As we repeatedly showed liquid film generation *via* plug instillation in our previous studies[49,51] and this current study, it is expected that air–liquid interface can be effectively created within the *in vitro*-cultured trachea *via* intratracheal liquid plug instillation. Because topically seeded cells can be washed away by instilled liquid plugs, however, the plug instillation would need to be initiated after the seeded cells can adhere and engraft firmly onto the de-epithelialized airway lumen.[75] The initiation timing and flow conditions of the liquid instillation to establish the air–liquid interface can be determined experimentally.

The impact of the current study can be further improved by demonstrating reestablishment of the functional airway epithelium and by creating diseased airway models following de-epithelialization. In this current study, however, the goal is to create an imaging-coupled bioreactor and establish a tissue manipulation methodology that can synergistically allow *in vitro* generation and culture of de-epithelialized airway tissues. Accordingly, *in vitro* investigations on regeneration of the intrinsic epithelial barrier function and modeling of human lung diseases (*e.g.*, lung fibrosis) could be an immediate important application of this study. In such studies, reestablishment of the airway epithelial barrier with restored native mucociliary flow, tight-junctions, and cell polarization can be studied in both healthy and disease states. Towards this goal, rigorous characterizations would be needed to quantify biological and structural similarities between the *in vitro*-cultured de-epithelialized tissues and *in vivo* airway tissues of live animals. Because differentiation, proliferation, and functional regeneration of implanted cells are heavily dependent on the local environment,[76] the tissue characterizations would need to be focused on optimization of the de-epithelialization and tissue culture strategies to maximize preservation of the native tissue matrix and cellular components.

Further, the gentle de-epithelialization methodology can be modified and potentially translated into clinics for "stem cell implantation therapy". For example, diseased or severely injured airway epithelium could be cleared from the airway tissue and patient-derived basal stem cells can be topically seeded to restore functional airway tissue. To translate this method, more rigorous studies will be required to determine the optimal concentration, amount, and incubation time of the de-epithelialization reagents (*e.g.*, detergents, enzymes, *etc.*) within the geometrically complex human respiratory tract.[50] The ability to locally deliver and monitor biochemical reagents or cells within the lung will be imperative to maximize the outcome of cell replacement therapy. Moreover, the *in situ* micro-imaging modality developed in this study could serve as a translational tool to evaluate newly delivered cells following therapeutic cell replacement in patients with airway disease.

Conclusions

In vitro airway tissue constructs created in the laboratory can facilitate fundamental studies of stem cell differentiation, development of effective therapeutic materials, and investigation of initiation and resolution of respiratory disorders. Here, we presented an imaging-assisted bioreactor platform and tissue manipulation methodology that allow partial removal of the endogenous tracheal epithelium, topical implantation of exogenous cells, and subsequent *in vitro* culture of the *ex vivo* tissues for an extended period. In addition, the platform and modalities created in this study can contribute to expanding our knowledge of the dynamic interactions between implanted exogenous cells and native airway ECM by allowing precise modulation of culture conditions and *in situ* assessment of the cell–tissue constructs. Further, the methodologies developed can be potentially translated into the clinics following additional validations and refinements to accelerate establishment of

stem cell-based treatments for lung diseases caused by dysfunctional airway epithelium.

Methods

Isolation and preparation of rat tracheas

In this study, tracheas isolated from Sprague-Dawley rats were used (total: 24 rats; weight: 250–270 g; SAS SD Rats, Charles River Laboratories). All procedures were performed in accordance with the animal welfare guideline and regulations of the Institute for Animal Care and Use Committee (IACUC) at Stevens Institute of Technology. Prior to lung isolation, the rats were anesthetized *via* inhalation of 2.5% isoflurane for 20 minutes using a vaporizer (SomnoSuite®, Kent Scientific). To prevent blood clotting in the pulmonary vasculature, 1000 unit per mL heparin (1 mL) was injected through the lateral tail vein and euthanized the animal using an overdose of 5% isoflurane. Immediately after euthanasia, the trachea was cannulated using a tracheal cannula (diameter: 2 mm; Cat. No. 73-2727, Harvard Apparatus). Midline thoracotomy was performed to isolate the trachea from the animal. The trachea was washed with 20 mL of 1× PBS at room temperature and was transferred into our custom-built bioreactor supplemented with culture medium containing Dulbecco's modified Eagle's medium (DMEM; Gibco™, Cat. No. 11965118, Thermo Fisher Scientific), recombinant human FGF-basic (Cat. No. 100-18B, PeproTech), fetal bovine serum (FBS; Gibco™, Cat. No. 10082147, Thermo Fisher Scientific), and antibiotic–antimycotic (Cat. No. 15240062, Thermo Fisher Scientific). The culture medium was used for both *in vitro* culture of cells and trachea tissues in this study.

Construction and assembly of the trachea bioreactor

We created a rat trachea bioreactor for de-epithelialization and *in vitro* culture of the rat trachea. The bioreactor consisted of a trachea culture chamber (dimension: 2.5 cm × 2.5 cm × 1.5 cm; total volume: 9.4 mL) in which the isolated trachea was placed for de-epithelialization and subsequent *ex vivo* culture. The culture chamber was fabricated by machining autoclavable Teflon® PTFE plastic (McMaster-Carr) using a computer numerical control (CNC) machine (Mini-Mill 3, Minitech®). Within the chamber, each end of the trachea was securely connected to a Luer cannula (diameter: 1.5 mm; Cat. No. EW-45501-30, Cole-Parmer) using sterilized surgical thread (size: 4; Matrix Wizard) to prevent leakage of reagents or cells introduced into the trachea interior. A multi-way connector was attached to the inlet cannula to apply different fluids and reagents to the trachea, such as detergent, washing solution, and culture medium using a syringe pump (cat. no. AL-4000, World Precision Instruments). To the outlet cannula, a *Y*-connector was attached to collect waste solution *via* one arm and to introduce a GRIN imaging probe for visualizing the inner surface of the trachea *via* the other arm of the connector. A transparent acrylic plastic sheet (McMaster-Carr) was cut and attached to the top of the main chamber using button head screws (10–32 threads, diameter 4.76 mm, length: 3.175 cm; McMaster-Carr).

Tracheal epithelium labeling

To enhance the visibility of the tracheal epithelium, the inner lumen of the trachea was labeled fluorescently using carboxyfluorescein succinimidyl ester (CFSE) cell labeling kit (ab113853, Abcam). The tissue labeling was performed according to the company's instruction prior to the de-epithelialization of the trachea. Briefly, CFSE was reconstituted in dimethyl sulfoxide (DMSO) and added with 1× PBS to the final concentration of 100 μM. Then, 1 mL of the CFSE solution was injected into the inner lumen of the trachea. The trachea was incubated for 10 min at 37 °C and then washed with 1× PBS (volume: 10 mL) three times to remove non-incorporated CFSE from the luminal surface. Our custom-built imaging device was used for *in situ* monitoring of the CFSE-labelled epithelial cells (excitation/emission: 492 nm/518 nm).

Custom-built micro-optical imaging device

To visualize the inner lumen of the trachea either in bright field or fluorescence, we built a micro-optical imaging device that could be integrated with the bioreactor. The imaging device comprised of a GRIN lens (diameter: 500 μm; SELFOC®, NSG Group), a scientific camera (PCO Panda 4.2), an achromatic doublet (AC254-150-A-ML, Thorlabs), a filter lens (ET535/50 m, Chroma®), a dual-edge super-resolution dichroic mirror (DI03-R488, Semrock), and a 20× objective lens (UCPLFLN20×, Olympus). For imaging the tracheal lumen, the distal end of the GRIN lens was inserted into the Luer connector that was attached to one end of the trachea. The light signals emitted from the luminal surface of the trachea were detected at the proximal end of the lens, which were then visualized *via* the camera. For fluorescent imaging, a laser light (wavelength: 488 nm, power: 150 mW; MDL-D-488-150 mW, Opto Engine) was passed into the imaging probe to excite the CFSE-labelled epithelium. Fluorescent light signals generated from the CFSE (emission wavelength: 515 nm) were filtered by the dichroic mirror and bandpass filter lens, then collected and imaged *via* the camera. The resolution of the imaging device was evaluated using a test target (1951 United States Air Force Resolution Test Target, Cat. No. R1DS1P, Thorlabs).

Construction of an electromagnetic shaker

To facilitate the detachment of epithelial cells from the tracheal lumen, we constructed an electromagnetic shaker, onto which a trachea-loaded bioreactor can be placed and mechanically oscillated at a specified frequency and amplitude. The custom-built shaker was composed of a subwoofer speaker (RSS21OHO-4, Dayton Audio) and a subwoofer plate amplifier (SPA250DSP, Dayton Audio). A rigid acrylic plate (dimensions: 25 cm × 30 cm × 1.5 cm;

McMaster-Carr) was attached onto the diaphragm of the speaker (diameter: 21 cm). The trachea bioreactor was loaded on the plate during mechanical oscillation. The frequency and amplitude of the shaker were manipulated by feeding a computer-generated sinusoidal waveform to the shaker. The response of the shaker was measured using an accelerometer (IIS3DWBTR, STMicroelectronics) or a high-frame-rate camera (240 frames per second; iPhone 11 Pro).

De-epithelialization of *in vitro*-cultured rat trachea

To remove the epithelium from the *in vitro*-cultured rat trachea, an aqueous solution of sodium dodecyl sulfate (SDS; concentrations: 2% or 4%; Cat. No. 97064-472, VWR) was instilled directly into the trachea *via* an inlet cannula. Specifically, a small volume (50 μL) of either 2% or 4% SDS solution was infused through the trachea using a programmable syringe pump (flow rate: 6.3 mL s^{-1}; AL-4000, World Precision Instruments) to generate a thin film of the detergent solution on the luminal surface of the trachea.[49,51] To promote de-epithelization, the trachea was incubated in the bioreactor for 20 min at 37 °C. The bioreactor was then mechanically vibrated using our custom-built shaker at 20 Hz of frequency while being washed with 1× PBS solution three times (volume: 500 μL; flow rate: 10 mL s^{-1}).

Histological analysis

All tracheas, native and de-epithelialized, were fixed in 4% neutral buffered paraformaldehyde solution in 1× PBS (pH level: 7.4) at 4 °C overnight and transferred to a 70% ethanol solution. The fixed tracheas were then dehydrated in a series of isopropyl alcohol solutions (IPA; concentrations: 80, 90, 95, and 100%) and Citrisolv™ solution (Cat. No. 1061, Decon) prior to paraffin embedding. The paraffin-embedded trachea tissues were cut into thin slices (thickness: 5–8 μm) and were deparaffinized using Citrisolv™ solution followed by rehydration in a series of IPA solutions (concentrations: 100, 95, 90, 80, 70, 50%). For microscopic assessment of the tissue layers, the tissue sections were stained for hematoxylin and eosin (H&E), Masson's trichrome, and Movat's pentachrome at the Department of Molecular Pathology at Columbia University.

Immunofluorescence analysis

The paraffin-embedded trachea sections were deparaffinized with Citrisolv™ and rehydrated in serial concentrations of 100 to 50% IPA solutions. To retrieve the antigens, the tissue section samples were treated with boiling citrate buffer at pH 6. The samples were then permeabilized in 1× PBS with 0.25% Triton™ X-100 (Cat. No. 97063-864, VWR) and FBS for 20 min. The tissue sections were then blocked in 10% FBS for additional 2 hours at room temperature and stained by incubating primary antibodies (Table S2†) in a staining buffer containing 5% FBS and 1× PBS at 4 °C overnight. The tissue sections were then washed three times in washing buffer and stained with corresponding secondary antibodies (Table S3†). Lastly, the sections were washed, incubated with DAPI solution (4′,6-diamidino-2-phenylindole; ab228549, Abcam) for 15 min, rewashed, and mounted with mounting medium (Permount™, Cat. No. SP15-100, Fisher Chemical) for better preservation.

Glycosaminoglycan (GAG) and DNA quantifications

Sulfated glycosaminoglycans (sulfated GAGs) were quantified using the GAG Assay Kit (Cat. No. 6022, Chondrex) according to the manufacturer's protocol. Briefly, an isolated trachea sample was weighed and digested in papain solution (concentration: 125 μg mL^{-1}; Cat. No. 60224, Chondrex®) at 60 °C overnight. The absorbance of the solution was measured at 525 nm using a microplate reader (Synergy HTX multi-mode reader, BioTek™), and the measured values were normalized to the wet weight of the tissue sample. Similarly, DNA contents were measured using the Quant-it PicoGreen double-stranded DNA Kit (Quant-iT™ PicoGreen™ dsDNA assay kit, Cat. No. P7589, Invitrogen). Briefly, tissue isolate was digested in papain solution (concentration: 125 μg mL^{-1}) for 4 hours at 60 °C and the fluorescence intensity of the solution was measured (excitation/emission: 480 nm/530 nm) using the microplate reader. A standard calibration curve was produced by bacteriophage lambda DNA to quantify the DNA content in the solution.

Scanning electron microscopy (SEM)

The luminal surfaces of the tracheas were visualized *via* scanning electron microscopy (SEM). Both native (control) and de-epithelialized tracheas were cut into small tissue samples (length: ~5 mm), which were then fixed in 2.5% glutaraldehyde at pH 7.4 at 4 °C overnight. The fixed tissues were washed three times in 1× PBS and dehydrated in graded series of aqueous ethanol solutions (concentrations: 35, 50, 70, 85, 95, and 100% v/v). The tissues were kept in hexamethyldisilazane solvent (HMDS, Cat. No. AC120585000, Fisher Scientific) and air-dried overnight. The dried tissues were coated with gold using a sputter coater (EM MED020, Leica) which were then imaged using a scanning electron microscope (SEM; Auriga 40, Zeiss) with an accelerating voltage of 2 kV.

Tissue porosity and pore size analysis

The pore sizes and porosity of the de-epithelialized airway lumen were quantified by analyzing the SEM images. This was accomplished by using the "Analyze Particle" function of ImageJ software (NIH). The SEM images of the native (control) and de-epithelialized airway tissues were converted into binary images and the pores and intact tissue regions were separated within the images by adjusting the threshold values. Then, the pore size distribution and porosity percentage were determined by characterizing individual pores *via* ImageJ.

Labeling MSCs with quantum dots and *in vitro* imaging

To label the MSCs with quantum dots, approximately 10^7 cells were incubated with the quantum dots (emission wavelength: 655 nm; cat. No. Q21321MP, Thermo Fisher Scientific) in 2 mL of culture medium at room temperature for 1 h. The labeled cells were then washed with 1× PBS three times to remove unincorporated quantum dots. For the imaging, the quantum dot-labeled cells were resuspended in culture medium (cell concentration: 10^6 cell mL^{-1}). A small drop (volume: 100 μL) of the cell-suspended medium was placed on a glass slide and the individual cells were visualized using a GRIN lens that was vertically positioned above the cell drop under excitation with 488 nm laser.

Chondrocyte viability

To assess the viability of chondrocytes after de-epithelization and long-term culture, native (control) and de-epithelized tracheas (treated with 4% SDS solution) were cultured for two weeks in the bioreactor. After de-epithelialization, the luminal and exterior surfaces of the trachea were rinsed with the complete culture medium. The bioreactor was then transferred into an incubator at 37 °C and 5% CO_2. The culture medium in the trachea lumen and within the chamber was refreshed *via* a syringe pump (flow rate: 5 mL h^{-1}; volume: 10 mL; AL-4000, World Precision Instruments) and a programmable pump (flow rate: 5 mL min^{-1}; L/S® standard digital pump system, Cole-Parmer), respectively, every day. After two weeks, the trachea was sectioned and stained with live/dead reagent staining (LIVE/DEAD™ Viability/Toxicity Kit, Cat. No. L3224 Invitrogen) according to manufacturer instruction. Briefly, the trachea samples were cut into slices (thickness ~500 μm) and then incubated in 1 mL 1× PBS containing 10 μM calcein AM and 20 μM ethidium homodimer-1 (EthD-1) for 15 min. After incubation, 1× PBS was used to rinse the samples. A fluorescent microscope (D-Eclipse C1, Nikon) equipped with fluorescent optical filters with excitation/emission of 495 nm/515 nm for live cells and excitation/emission of 495 nm/635 nm for dead cells was used to assess the viability of cartilage in de-epithelialized tracheas.

Cytotoxicity evaluation of the de-epithelialized trachea

To evaluate the cytotoxicity of the de-epithelialized tracheas, mesenchymal stem cells (MSCs) were seeded and cultured on the luminal surface of the tracheas in the bioreactor. Survival and growth of the seeded cells were assessed during one week of *in vitro* culture. To do this, the de-epithelialized rat trachea treated with 4% SDS solution in the bioreactor was rinsed thoroughly using the culture medium. Next, the CFSE-labeled MSCs were suspended in the cell culture medium (cell concentration: 50 000 cells per mL; volume: 100 μL) were introduced into the trachea to deposit the cells onto the luminal surface. The trachea-loaded bioreactor was then placed in a gas-controlled cell incubator (MCO-20AIC, Panasonic) to culture the cell-seeded trachea at 37 °C and 5% CO_2 for 1, 4, or 7 days. During the cell culture, the culture medium within the inner space of the trachea was replaced with the fresh medium once a day using a programmable syringe pump (flow rate: 5 mL h^{-1}; volume: 10 mL; AL-4000, World Precision Instruments) and the removed culture medium was collected in a waste reservoir. In the meantime, the culture medium within the tissue culture chamber of the bioreactor was replaced continuously by circulating the medium between a reservoir and the chamber using a peristaltic pump (flow rate: 5 mL min^{-1}; L/S® standard digital pump system, Cole-Parmer). The culture medium in the reservoir (total volume: 50 mL) was replaced once in two days. Viability and proliferation of the trachea seeded with CFSE-labelled MSCs were evaluated following 1, 4, or 7 days of *in vitro* culture by measuring fluorescence signal emitted from the cells (excitation/emission: 492 nm/518 nm) using a fluorescent microscope (Eclipse E1000, Nikon) or our micro-imaging device.

Study design and statistical analysis

We present all data as mean ± standard deviation (SD). All experiments were conducted at least three times to ensure reproducibility of the results and to evaluate statistical significance within each experimental group. The de-epithelialized tracheas were compared with healthy native trachea freshly isolated from Sprague-Dawley rats. One-way analysis of variance (one-way ANOVA) was used following by Tukey's honest significant *post hoc* test to compare the means of control groups. We considered a difference statistically significant if $p < 0.05$.

Author contributions

S. M. M., J. C., and J. K. conceived the concept of this work. S. M. M., J. C., and J. K. designed the experiments. S. M. M. and J. C. performed the experiments. S. M. M., J. C., M. R. P., J. D. O., S. X. L. H., G. V. N., and J. K. analyzed the results. S. M. M., M. R. P., J. D. O., G. V. N., and J. K. wrote the manuscript.

Conflicts of interest

The authors declare that they have no known competing financial interests or personal relationships that could have appeared to influence the work reported in this paper.

Acknowledgements

This research has been supported in part by American Thoracic Society Foundation Research Program, Research Grants from New Jersey Health Foundation, and the National Science Foundation (CAREER Award 2143620) provided to J. K. and the National Institutes of Health (P41 EB027062) to G. V. N. The authors would like to thank Drs. Tsengming (Alex) Chou and Matthew Libera, and Mr. Xinpei Wu at Stevens Laboratory for Multiscale Imaging (LMSI) for their assistance with SEM imaging of the tissue samples.

References

1 F. Li, J. He, J. Wei, W. C. Cho and X. Liu, *Stem Cells Int.*, 2015, **2015**, 728307.
2 R. E. Rayner, P. Makena, G. L. Prasad and E. Cormet-Boyaka, *Sci. Rep.*, 2019, **9**, 500.
3 C. H. Dean and R. J. Snelgrove, *Am. J. Respir. Crit. Care Med.*, 2018, **198**, 1355–1356.
4 R. G. Crystal, S. H. Randell, J. F. Engelhardt, J. Voynow and M. E. Sunday, *Proc. Am. Thorac. Soc.*, 2008, **5**, 772–777.
5 A. Wanner, M. Salathé and T. G. O'Riordan, *Am. J. Respir. Crit. Care Med.*, 1996, **154**, 1868–1902.
6 C. Coraux, R. Hajj, P. Lesimple and E. Puchelle, *Eur. Respir. Rev.*, 2005, **14**, 131.
7 A. R. Berkebile, J. A. Bartlett, M. Abou Alaiwa, S. M. Varga, U. F. Power and P. B. McCray, *Am. J. Respir. Cell Mol. Biol.*, 2019, **62**, 104–111.
8 M. Cohen-Cymberknoh, E. Kerem, T. Ferkol and A. Elizur, *Thorax*, 2013, **68**, 1157.
9 J. Mianné, E. Ahmed, C. Bourguignon, M. Fieldes, I. Vachier, A. Bourdin, S. Assou and J. De Vos, *Am. J. Respir. Cell Mol. Biol.*, 2018, **59**, 672–683.
10 E. Roscioli, R. Hamon, S. E. Lester, H. P. A. Jersmann, P. N. Reynolds and S. Hodge, *Respir. Res.*, 2018, **19**, 234.
11 N. T. N. Trinh, O. Bardou, A. Privé, E. Maillé, D. Adam, S. Lingée, P. Ferraro, M.-Y. Desrosiers, C. Coraux and E. Brochiero, *Eur. Respir. J.*, 2012, **40**, 1390.
12 A. Horani and T. W. Ferkol, *Chest*, 2018, **154**, 645–652.
13 C. H. Hochberg and V. K. Sidhaye, in *Lung Epithelial Biology in the Pathogenesis of Pulmonary Disease*, ed. V. K. Sidhaye and M. Koval, Academic Press, Boston, 2017, pp. 165–184.
14 K. H. Benam, R. Villenave, C. Lucchesi, A. Varone, C. Hubeau, H.-H. Lee, S. E. Alves, M. Salmon, T. C. Ferrante, J. C. Weaver, A. Bahinski, G. A. Hamilton and D. E. Ingber, *Nat. Methods*, 2016, **13**, 151–157.
15 S. E. Gilpin, J. M. Charest, X. Ren and H. C. Ott, *Thorac. Surg. Clin.*, 2016, **26**, 163–171.
16 M. Z. Nikolić, O. Caritg, Q. Jeng, J. A. Johnson, D. Sun, K. J. Howell, J. L. Brady, U. Laresgoiti, G. Allen, R. Butler, M. Zilbauer, A. Giangreco and E. L. Rawlins, *eLife*, 2017, **6**, e26575.
17 B. F. Niemeyer, P. Zhao, R. M. Tuder and K. H. Benam, *SLAS Discovery*, 2018, **23**, 777–789.
18 K. B. McCauley, F. Hawkins, M. Serra, D. C. Thomas, A. Jacob and D. N. Kotton, *Cell Stem Cell*, 2017, **20**, 844–857. e846.
19 R. Plebani, R. Potla, M. Soong, H. Bai, Z. Izadifar, A. Jiang, R. N. Travis, C. Belgur, M. J. Cartwright, R. Prantil-Baun, P. Jolly, S. E. Giplin, M. Romano and D. E. Ingber, *medRxiv*, 2021, DOI: 10.1101/2021.07.15.21260407.
20 L. E. Haswell, K. Hewitt, D. Thorne, A. Richter and M. D. Gaça, *Toxicol. In Vitro*, 2010, **24**, 981–987.
21 C. Xiao, S. M. Puddicombe, S. Field, J. Haywood, V. Broughton-Head, I. Puxeddu, H. M. Haitchi, E. Vernon-Wilson, D. Sammut, N. Bedke, C. Cremin, J. Sones, R. Djukanović, P. H. Howarth, J. E. Collins, S. T. Holgate, P. Monk and D. E. Davies, *J. Allergy Clin. Immunol.*, 2011, **128**, 549–556.e512.
22 A. Jacob, M. Morley, F. Hawkins, K. B. McCauley, J. C. Jean, H. Heins, C. L. Na, T. E. Weaver, M. Vedaie, K. Hurley, A. Hinds, S. J. Russo, S. Kook, W. Zacharias, M. Ochs, K. Traber, L. J. Quinton, A. Crane, B. R. Davis, F. V. White, J. Wambach, J. A. Whitsett, F. S. Cole, E. E. Morrisey, S. H. Guttentag, M. F. Beers and D. N. Kotton, *Cell Stem Cell*, 2017, **21**, 472–488.e410.
23 A. Strikoudis, A. Cieślak, L. Loffredo, Y.-W. Chen, N. Patel, A. Saqi, D. J. Lederer and H.-W. Snoeck, *Cell Rep.*, 2019, **27**, 3709–3723.e3705.
24 E. Schruf, V. Schroeder, H. Q. Le, T. Schönberger, D. Raedel, E. L. Stewart, K. Fundel-Clemens, T. Bluhmki, S. Weigle, M. Schuler, M. J. Thomas, R. Heilker, M. J. Webster, M. Dass, M. Frick, B. Stierstorfer, K. Quast and J. P. Garnett, *FASEB J.*, 2020, **34**, 7825–7846.
25 H. Surendran, S. Nandakumar and R. Pal, *Stem Cells Dev.*, 2020, **29**, 1365–1369.
26 S. X. Huang, M. N. Islam, J. O'Neill, Z. Hu, Y. G. Yang, Y. W. Chen, M. Mumau, M. D. Green, G. Vunjak-Novakovic, J. Bhattacharya and H. W. Snoeck, *Nat. Biotechnol.*, 2014, **32**, 84–91.
27 A. J. Miller, B. R. Dye, D. Ferrer-Torres, D. R. Hill, A. W. Overeem, L. D. Shea and J. R. Spence, *Nat. Protoc.*, 2019, **14**, 518–540.
28 F. J. Hawkins, S. Suzuki, M. L. Beermann, C. Barillà, R. Wang, C. Villacorta-Martin, A. Berical, J. C. Jean, J. Le Suer, T. Matte, C. Simone-Roach, Y. Tang, T. M. Schlaeger, A. M. Crane, N. Matthias, S. X. L. Huang, S. H. Randell, J. Wu, J. R. Spence, G. Carraro, B. R. Stripp, A. Rab, E. J. Sorsher, A. Horani, S. L. Brody, B. R. Davis and D. N. Kotton, *Cell Stem Cell*, 2021, **28**, 79–95.e78.
29 P. Duchesneau, T. K. Waddell and G. Karoubi, *Int. J. Mol. Sci.*, 2020, **21**, 5219.
30 B. A. Guenthart, J. D. O'Neill, J. Kim, K. Fung, G. Vunjak-Novakovic and M. Bacchetta, *J. Heart Lung Transplant.*, 2019, **38**, 215–224.
31 L. Van Haute, G. De Block, I. Liebaers, K. Sermon and M. De Rycke, *Respir. Res.*, 2009, **10**, 105.
32 S. Halldorsson, V. Asgrimsson, I. Axelsson, G. H. Gudmundsson, M. Steinarsdottir, O. Baldursson and T. Gudjonsson, *In Vitro Cell. Dev. Biol.: Anim.*, 2007, **43**, 283–289.
33 H. Lin, H. Li, H.-J. Cho, S. Bian, H.-J. Roh, M.-K. Lee, J. S. Kim, S.-J. Chung, C.-K. Shim and D.-D. Kim, *J. Pharm. Sci.*, 2007, **96**, 341–350.
34 J. C. Nawroth, R. Barrile, D. Conegliano, S. van Riet, P. S. Hiemstra and R. Villenave, *Adv. Drug Delivery Rev.*, 2019, **140**, 12–32.
35 K. Gkatzis, S. Taghizadeh, D. Huh, D. Y. R. Stainier and S. Bellusci, *Eur. Respir. J.*, 2018, **52**, 11800876.
36 D. Huh, H. J. Kim, J. P. Fraser, D. E. Shea, M. Khan, A. Bahinski, G. A. Hamilton and D. E. Ingber, *Nat. Protoc.*, 2013, **8**, 2135–2157.
37 L. Si, H. Bai, M. Rodas, W. Cao, C. Y. Oh, A. Jiang, R. Moller, D. Hoagland, K. Oishi, S. Horiuchi, S. Uhl, D. Blanco-Melo,

R. A. Albrecht, W.-C. Liu, T. Jordan, B. E. Nilsson-Payant, I. Golynker, J. Frere, J. Logue, R. Haupt, M. McGrath, S. Weston, T. Zhang, R. Plebani, M. Soong, A. Nurani, S. M. Kim, D. Y. Zhu, K. H. Benam, G. Goyal, S. E. Gilpin, R. Prantil-Baun, S. P. Gygi, R. K. Powers, K. E. Carlson, M. Frieman, B. R. tenOever and D. E. Ingber, *Nat. Biomed. Eng.*, 2021, **5**, 815–829.

38 K. H. Benam, M. Mazur, Y. Choe, T. C. Ferrante, R. Novak and D. E. Ingber, *Methods Mol. Biol.*, 2017, **1612**, 345–365.

39 K. Hajipouran Benam, R. Novak, R. Villenave, C. Lucchesi, C. Hubeau, J. Nawroth, M. Hirano-Kobayashi, T. C. Ferrante, Y. Choe, R. Prantil-Baun, J. C. Weaver, G. A. Hamilton, A. Bahinski and D. E. Ingber, *Eur. Respir. J.*, 2016, **48**, OA4542.

40 L. G. Griffith and M. A. Swartz, *Nat. Rev. Mol. Cell Biol.*, 2006, **7**, 211–224.

41 A. M. Greaney, T. S. Adams, M. S. Brickman Raredon, E. Gubbins, J. C. Schupp, A. J. Engler, M. Ghaedi, Y. Yuan, N. Kaminski and L. E. Niklason, *Cell Rep.*, 2020, **30**, 4250–4265. e4256.

42 M. D. Green, S. X. Huang and H. W. Snoeck, *BioEssays*, 2013, **35**, 261–270.

43 C. R. Butler, R. E. Hynds, K. H. Gowers, H. Lee Ddo, J. M. Brown, C. Crowley, V. H. Teixeira, C. M. Smith, L. Urbani, N. J. Hamilton, R. M. Thakrar, H. L. Booth, M. A. Birchall, P. De Coppi, A. Giangreco, C. O'Callaghan and S. M. Janes, *Am. J. Respir. Crit. Care Med.*, 2016, **194**, 156–168.

44 M. J. Goldman, Y. Yang and J. M. Wilson, *Nat. Genet.*, 1995, **9**, 126–131.

45 D. W. Borthwick, M. Shahbazian, Q. T. Krantz, J. R. Dorin and S. H. Randell, *Am. J. Respir. Cell Mol. Biol.*, 2001, **24**, 662–670.

46 R. Hajj, T. Baranek, R. Le Naour, P. Lesimple, E. Puchelle and C. Coraux, *Stem Cells*, 2007, **25**, 139–148.

47 S. X. L. Huang, M. D. Green, A. T. de Carvalho, M. Mumau, Y.-W. Chen, S. L. D'Souza and H.-W. Snoeck, *Nat. Protoc.*, 2015, **10**, 413–425.

48 R. Nossa, J. Costa, L. Cacopardo and A. Ahluwalia, *J. Tissue Eng.*, 2021, **12**, 20417314211008696.

49 J. Kim, J. D. O'Neill, N. V. Dorrello, M. Bacchetta and G. Vunjak-Novakovic, *Proc. Natl. Acad. Sci. U. S. A.*, 2015, **112**, 11530–11535.

50 J. Kim, B. Guenthart, J. D. O'Neill, N. V. Dorrello, M. Bacchetta and G. Vunjak-Novakovic, *Sci. Rep.*, 2017, **7**, 13082.

51 J. Kim, J. D. O'Neill and G. Vunjak-Novakovic, *Appl. Phys. Lett.*, 2015, **107**, 144101.

52 R. G. Smock and R. Meijers, *Open Biol.*, 2018, **8**, 180026.

53 N. Afratis, C. Gialeli, D. Nikitovic, T. Tsegenidis, E. Karousou, A. D. Theocharis, M. S. Pavão, G. N. Tzanakakis and N. K. Karamanos, *FEBS J.*, 2012, **279**, 1177–1197.

54 J. M. Mattson, R. Turcotte and Y. Zhang, *Biomech. Model. Mechanobiol.*, 2017, **16**, 213–225.

55 J. Chen, S. M. Mir, M. R. Pinezich, J. D. O'Neill, B. A. Guenthart, M. Bacchetta, G. Vunjak-Novakovic, S. X. L. Huang and J. Kim, *ACS Biomater. Sci. Eng.*, 2022, **8**, 82–88.

56 J. L. Balestrini, A. L. Gard, A. Liu, K. L. Leiby, J. Schwan, B. Kunkemoeller, E. A. Calle, A. Sivarapatna, T. Lin, S. Dimitrievska, S. G. Cambpell and L. E. Niklason, *Integr. Biol.*, 2015, **7**, 1598–1610.

57 D. A. Taylor, L. C. Sampaio, Z. Ferdous, A. S. Gobin and L. J. Taite, *Acta Biomater.*, 2018, **74**, 74–89.

58 J. L. Balestrini, A. L. Gard, A. Liu, K. L. Leiby, J. Schwan, B. Kunkemoeller, E. A. Calle, A. Sivarapatna, T. Lin, S. Dimitrievska, S. G. Cambpell and L. E. Niklason, *Integr. Biol.*, 2015, **7**, 1598–1610.

59 L. M. Godin, B. J. Sandri, D. E. Wagner, C. M. Meyer, A. P. Price, I. Akinnola, D. J. Weiss and A. Panoskaltsis-Mortari, *PLoS One*, 2016, **11**, e0150966.

60 N. Qu, P. de Vos, M. Schelfhorst, A. de Haan, W. Timens and J. Prop, *J. Heart Lung Transplant.*, 2005, **24**, 882–890.

61 M. Zang, Q. Zhang, E. I. Chang, A. B. Mathur and P. Yu, *Plast. Reconstr. Surg.*, 2013, **132**, 549e–559e.

62 Z. Dimou, E. Michalopoulos, M. Katsimpoulas, D. Dimitroulis, G. Kouraklis, C. Stavropoulos-Giokas and P. Tomos, *Anticancer Res.*, 2019, **39**, 145–150.

63 S. Haykal, M. Salna, Y. Zhou, P. Marcus, M. Fatehi, G. Frost, T. Machuca, S. O. Hofer and T. K. Waddell, *Tissue Eng., Part C*, 2014, **20**, 681–692.

64 P. Hong, M. Bezuhly, M. E. Graham and P. F. Gratzer, *Int. J. Pediatr. Otorhinolaryngol.*, 2018, **112**, 67–74.

65 C. Li, A. Alfonso-Garcia, J. McMasters, J. Bec, B. Weyers, L. Uyesaka, L. Griffiths, A. Panitch and L. Marcu, *Methods Appl. Fluoresc.*, 2019, **7**, 044003.

66 A. Richardson, L. A. Schwerdtfeger, D. Eaton, I. McLean, C. S. Henry and S. A. Tobet, *Anal. Methods*, 2020, **12**, 297–303.

67 D. Mizokami, K. Araki, N. Tanaka, H. Suzuki, M. Tomifuji, T. Yamashita, Y. Ueda, H. Shimada, K. Matsushita and A. Shiotani, *PLoS One*, 2015, **10**, e0116279.

68 C. Leung, S. J. Wadsworth, S. J. Yang and D. R. Dorscheid, *Am. J. Physiol.*, 2020, **318**, L1063–L1073.

69 J. Kong, S. Wen, W. Cao, P. Yue, X. Xu, Y. Zhang, L. Luo, T. Chen, L. Li, F. Wang, J. Tao, G. Zhou, S. Luo, A. Liu and F. Bao, *Stem Cell Res. Ther.*, 2021, **12**, 95.

70 S. A. Taqi, S. A. Sami, L. B. Sami and S. A. Zaki, *J. Oral Maxillofac. Pathol.*, 2018, **22**, 279.

71 D. Le Bihan, *NMR Biomed.*, 1995, **8**, 375–386.

72 Y. H. Sniekers and C. C. van Donkelaar, *Biophys. J.*, 2005, **89**, 1302–1307.

73 L. Moraes, P. L. Silva, A. Thompson, C. L. Santos, R. S. Santos, M. V. S. Fernandes, M. M. Morales, V. Martins, V. L. Capelozzi, M. G. de Abreu, P. Pelosi and P. R. M. Rocco, *Front. Physiol.*, 2018, **9**, 1193–1206.

74 J. Chen, S. M. Mir, M. R. Pinezich, J. D. O'Neill, B. A. Guenthart, M. Bacchetta, G. Vunjak-Novakovic, S. X. L. Huang and J. Kim, *Acta Biomater.*, 2021, **131**, 370–380.

75 S. Suzuki, F. J. Hawkins, C. Barillà, M. L. Beermann, D. N. Kotton and B. R. Davis, *STAR Protoc.*, 2021, **2**, 100683.

76 B. R. Stripp and S. D. Reynolds, *Am. J. Respir. Cell Mol. Biol.*, 2005, **32**, 85–86.